Colloid and Interface Science Communications 48 (2022) 100621

Contents lists available at ScienceDirect

Colloid and Interface Science Communications

journal homepage: www.elsevier.com/locate/colcom

Rapid Communication

Development of porous silver nanoparticle/polycaprolactone/polyvinyl alcohol coatings for prophylaxis in titanium interconnected samples for dental implants

Ana Alcudia [a,*], Belén Begines [a,*], Paula Rodriguez-Lejarraga [a], Valeria Greyer [a], Vanda Cristina Fortio Godinho [b], Eloísa Pajuelo [c], Yadir Torres [b]

[a] Departamento de Química Orgánica y Farmacéutica, Facultad de Farmacia, Universidad de Sevilla, C/ Profesor García González, 2, 41012 Seville, Spain
[b] Departamento de Ingeniería y Ciencia de los Materiales y del Transporte, Escuela Politécnica Superior, Universidad de Sevilla, 41011 Seville, Spain
[c] Departamento de Microbiología y Parasitología, Facultad de Farmacia, Universidad de Sevilla, C/ Profesor García González, 2, 41012 Seville, Spain

ARTICLE INFO

Keywords:
Biopolymers
Silver nanoparticles
Antimicrobial activity
Ag^+ release
Porous titanium
Pharmaceutical applications

ABSTRACT

Stress shielding phenomenon, poor osseointegration, or bacterial infections of titanium dental implants are widely recognized as key problems that deeply affect their survival rate. In this work, a joint solution to solve these three limitations is proposed. The first two issues were minimized applying porous Ti samples. This substrate exhibits an appropriated biomechanical equilibrium (stiffness and mechanical resistance) and good biofunctionality (ability to promote bone ingrowth). On the other hand, the porous Ti disc was coated with biocompatible and non-toxic polymeric composites matrices using poly-ε-caprolactone and partially acetylated polyvinyl alcohol, combined with silver nanoparticles as a therapeutic antimicrobial agent. The optimization of the best blend composition and optimal nanoparticles concentration were investigated. Finally, the two composites with the best antimicrobial activity were infiltrated into porous Ti discs. The deposited coatings presented good adhesion and a honeycomb-like surface structure that could promote vascularization of the implant and enhance osseointegration.

1. Introduction

Dental implants are currently the preferred treatment for patients with missing teeth who need to reestablish masticatory function in addition to aesthetic appearance. Although they present a low failure rate (5–10%), the high number of implants placed throughout the year makes this percentage important and should be considered for the field of dental implantology. Most of the issues that end in implant loosening are related to stress shielding phenomenon, poor osseointegration, and bacterial infections. Furthermore, the success of the dental implant depends, on the one hand, on the quality and quantity of the host tissue and, on the other hand, on the intrinsic properties of the implanted materials and the biointerface between the implant and bone tissue [1]. Therefore, it is crucial to develop materials with suitable biomechanical properties (stiffness, mechanical and fatigue resistance) and biofunctional balance (corrosion resistance and bone ingrowth) that are simultaneously capable of managing and preventing the high rate of implant-related infections [2].

During the last decade, attention has been focused on the development of porous titanium materials with improved mechanical properties to mimic bone tissue and minimize the effective stress-shielding phenomenon [3,4]. In addition, space-holder methodology applied to implant production is a promising, convenient and affordable route that allows the preparation of porous materials showing promising results for osseointegration [5,6]. However, titanium is a metallic material with an optimal surface for bacteria to proliferate, with consequent infection-related problems for patients. An adequate surface coating could be a solution to mitigate the risk of infection, acting as a stable local drug delivery matrix system and, at the same time, improving implant biocompatibility or corrosion resistance [7]. In this sense, biodegradable, biocompatible, and non-toxic polymeric matrices, with a 'bonelike' surface, have already been proposed as degradable protective coatings [8] with potential for osseointegration and antibacterial function [9,10]. In particular, attention has been paid to the formation of three-

* Corresponding authors at: Departamento de Química Orgánica y Farmacéutica, Facultad de Farmacia, Universidad de Sevilla, C/ Profesor García González, 2, 41012 Seville, Spain.
E-mail addresses: aalcudia@us.es (A. Alcudia), bbegines@us.es (B. Begines).

https://doi.org/10.1016/j.colcom.2022.100621
Received 27 December 2021; Received in revised form 13 March 2022; Accepted 25 March 2022
Available online 12 April 2022

dimensional polymeric matrices or scaffolds, capable of mimicking the structure of biological tissues at macro-, micro-, and nanoscales [11].

From a material science point of view, coating metallic porous implants with polymeric materials presents several challenges that need to be addressed. It should present mechanical stability. Lack of adherence between the coating and the substrate and consequent detachment would alter the functionality of the coating. Furthermore, an antibacterial coating with a stable release profile of the therapeutic agent is desirable during the osseointegration period (at least 3 to 6 months). Therefore, the polymeric materials selected as the drug delivery matrix should possess a low degradation rate. In this sense, poly-ε-caprolactone (PCL) is a semicrystalline aliphatic polyester polymer, known for its good mechanical properties, biocompatibility, non-toxicity, and slow biodegradability [12,13]. PLC is a widely investigated, low-cost biomedical polymer with wound healing capacity, used for drug delivery and for the development of temporary 3D scaffolds in bone tissue engineering [13]. In fact, it is currently approved by the US Food and Drug Administration (FDA) for clinical use. However, PLC is intrinsically hydrophobic and cannot be easily connected to the bone natural tissue. This lack of wettability hampers cell attachment and spread [12,13]. The deficient bioactivity of PLC can be overcome by blending it with hydrophilic polymers like polyvinyl alcohol (PVA). It is a biodegradable polymer, highly compatible for blending with other biopolymers, presenting tunable mechanical properties with applications in 3D scaffolds for tissue engineering [9,10]. Because PVA is prepared by partial or complete hydrolysis of poly(vinyl acetate), it can be obtained with variable degrees of deacetylation. This fact plays an important role in the water solubility of this polymeric material. Previous studies have investigated the use of PCL/PVA composites in bone tissue engineering [14–17], mainly in the form of core-sheath fibrous scaffolds formed by electrospinning with the ability to deliver therapeutic agents in a controlled way. Unfortunately, the use of electrospinning to generate polymeric coatings hinders the access of the composite to the inner pores, although they are interconnected, which may drastically reduce implant integration in the bone.

On the other hand, the use of nanoparticles is being widely investigated today for their promising characteristics [18,19], especially as antimicrobial agents [20]. Their good stability, nanometric size, what entails a high surface-to-volume ratio, and potential surface modification confer them excellent antibacterial properties with low toxicity [20–23]. The application of nanoparticles as a drug to combat bacterial diseases would be an excellent alternative to the use of conventional antibiotics, avoiding the worldwide problem of antibiotic resistance [24]. Moreover, the prophylactic or therapeutic effects of Ag^{+} have been widely applied in the pharmaceutical field due to their damage to bacterial cells with low affection for animal cells [25]. Particularly, silver is known to have multiple activities against *S. aureus*, since it binds to 38 different proteins within the cell [26]. Besides, it induces the formation of reactive oxygen species and compromises the integrity of the membrane [27]. Similar mechanisms are reported for *P. aeruginosa* [28]. Therefore, AgNPs would be an excellent candidate as a novel therapeutic approach for antibacterial treatments.

In this research work, biocompatible and non-toxic composites based on PCL and PVA, combined with antimicrobial AgNPs, have been proposed as polymeric matrices to enhance the bioactivity of porous Ti substrates infiltrated with these composite materials. The optimal pore size and pore content of the Ti substrates will be fabricated employing the accessible space-holder technique, to allow adequate infiltration of the biomaterial, as well as minimization of stress shielding phenomenon, to avoid undesirable surrounding bone tissue resorption and promotion of osseointegration. A study of the optimal amount of AgNPs acting as antimicrobial therapeutic agents has been incorporated, looking for both short-term and long-term drug delivery release profiles combined with diverse proportions of PCL/PVA matrices. AgNPs/PCL/PVA biomaterials have been tested to evaluate their potential as effective antimicrobial agents against *Pseudomonas aeruginosa* and *Staphylococcus aureus*. The most promising biopolymer composites with best antimicrobial behavior in the short- or long-term have been infiltrated onto porous Ti discs to evaluate the total pore coverage and to demonstrate the potential of this methodology to fabricate implants with enhanced osseointegration and antibacterial properties.

2. Materials and methods

All chemicals were used as received without further purification. Polyethylene glycol 3000 (PEG 3000), polyethylene glycol 200 (PEG 200), polyvinyl alcohol (PVA, Mn = 30.000–70.000 g/mol, 87–90% hydrolyzed), poly-ε-caprolactone (PCL), glycerol and NH_4HCO_3 were obtained from Merck (Darmstadt, Germany). Dichloromethane was purchased from Honeywell (Badalona, Spain) and HCl, from Scharlau (Barcelona, Spain). Gentamicin discs (6 mm diameter) were obtained from Oxford 2000 Ltd. (Hampshire, United Kingdom). Tryptone soya broth (TSB) and Tryptone soya agar (TSA) were purchased from Intron Biotechnology (Burlington, MA, United States). Also, Ti powders (c.p. Ti–Grade IV, provided by SEJONG Materials Co. Ltd.) were obtained via hydrogenation/dehydrogenation, presenting irregular morphology and a particle size distribution of 9.7 μm (<10%), 23.3 μm (<50%) and 48.4 μm (<90%).

2.1. Porous Ti substrate preparation and characterization

Porous Ti substrates were fabricated by the space-holder technique. Titanium powder is mixed with 50% volume of ammonium bicarbonate (NH_4HCO_3, 250–350 μm particle size range), during 40 min using a Turbula T2C Shaker-Mixer (tmg machines, Birmingham, U.K.), to ensure good homogenization [29]. Green compacts were produced in a universal Instron 5505 testing machine (Instron, High Wycombe, UK) by pressing at 800 MPa. The spacers were thermally removed by heat treating the compacts in two stages of 12 h at 60 and 110°C, respectively, under low vacuum conditions of 10^{-2} mbar. A final sintering step was carried out at 1250°C in a molybdenum chamber furnace (Termolab–Fornos Eléctricos, Lda., Águeda, Portugal) under high vacuum atmosphere (~10^{-5} mbar) for 2 h. Before coating, the surfaces of the disc (both the top surface and the cross-section) were ground and polished with magnesium oxide (MgO) and hydrogen peroxide (H_2O_2). The porosity fraction, size, and morphology of the pores were preserved after polishing. The final substrate dimensions were 12 mm diameter and 4 mm height.

The porosity of the substrates was studied by Archimedes' method for the determination of the density, total, and interconnected porosity (ρ, P_T, and P_i, respectively) [30]. Furthermore, the porous substrates were analyzed by image analysis (IA) to measure the equivalent diameter (D_{eq}) and the shape factor (F_f), using a Nikon Epiphot optical microscope (Nikon, Tokyo, Japan) coupled with a Jenoptik Progres C3 camera (Jenoptik, Jena, Germany) and Image-Pro Plus 6.2 analysis software. On the other hand, in terms of macro-mechanical behavior, the substrates were subjected at a uniaxial compression test in an Instron 5505 universal testing machine [31–33], in order to evaluate the yield strength (σ_y). Finally, the dynamic Young's modulus (E_d) were obtained using ultrasound technique (KRAUTKRAMER USM 35 equipment) [34,35].

2.2. Synthesis of composite materials

AgNPs were synthesized according to the method of Madhavan et al. [36], obtaining nanoparticles with similar characteristics (approximately 20 nm and spherical shape). Briefly, 10 mL of PEG 200 was stirred with 3.42 g of PEG 3000 at 80°C. When it was completely dissolved, the temperature was set at 40°C and 100 mg of silver nitrate was added to obtain a brown solution.

Composites were synthesized by mixing two commercial polymers, PVA and PCL, with the silver nanoparticles previously described.

Different PCL/PVA ratios (100/0, 90/10; 80/20; 70/30; 50/50 and 40/60) were used to obtain 2 g of the final blend. For this purpose, under stirring, the relevant amount of PVA was weighed and dissolved in dichloromethane, then PCL was added until total dissolution. Subsequently, AgNPs were added in different weight ratios, in terms of the weight of the mixture (0.0125%; 0.025%; 0.05%; 0.1%; 0.2%; 0.3% and 0.4% w/w of silver), to the different combinations of the blend. The obtained mixed was poured into a crystallizer dish, and dried for one day at 37°C.

2.3. Zone of inhibition testing

Reference strains of gram-negative bacteria, *Pseudomonas aeruginosa* (*P. aeruginosa*, ATCC 15692), and gram-positive bacteria, *Staphylococcus aureus* (*S. aureus*, ATCC 29737), were used to test the antimicrobial activity of the composites. Both strains were retrieved from the Spanish culture collection (University of Valencia)

All different combinations of composites were cut to obtain approximately 8 mm diameter cylinders and tested in triplicate for each strain. Antibacterial activity studies were conducted using the modified Kirby-Bauer disk diffusion method [37]. Briefly, an isolated colony of each strain was cultured in TSB. Inoculum with a volume of 100 or 150 μL of *P. aeruginosa* or *S. aureus*, respectively, was streaked on TSA agar plates to form a bacterial lawn. The samples were deposited on top of the TSA, including a gentamicin disc in the center of the plate, as a positive control. Finally, the Petri dishes were incubated for 24 h at 37°C and the diameter of the inhibition was measured and used to compare the antibacterial efficacy of the different composites. Although all the samples were tested in triplicate, the number of halo measurements were 9 since 3 measurements of diameter were taken from each sample (horizontal, vertical and diagonal). To standardize the measurements of the halos, the diameter of the halo was divided by the diameter of the composite.

2.4. Silver release detection

To quantify the amount of silver cations released by the various composites at different time intervals, 2 g of the material was cut and immersed in 10 mL of Milli-Q water. After the pre-established time on an orbital shaker (Heidolph Unimax 1010, Heidolph Instruments, Schwabach, Germany) at 135 rpm and 37°C, the supernatant was removed, and 1 mL aliquot was taken. To the extracted aliquot, 1 mL of 1 M HCl solution was added to generate an AgCl precipitate. A UV–Vis Shimadzu UV-1280 spectrophotometer (Shimadzu Corporation, Kyoto, Japan) was used for precipitate detection, wavelength of 480 nm. 10 mL of fresh Milli-Q water was added, and the same method was repeated at different times: 1, 2, 4, 6, and 24 h, and 2, 3, 4, 7, 10, 14 and 21 days. Silver ions released from the different samples were estimated using a calibration line obtained from known concentrations of $AgNO_3$ (Fig. S1).

2.5. Infiltration on porous titanium substrate

The most promising composites exhibiting the best characteristics from the antimicrobial activity point of view were infiltrated onto the substrates by dropwise suspension deposition, adding 150 μL of the composite suspension, and deposited on the titanium substrate, using a heat shrink tube to ensure that the entire solution penetrated. These substrates were previously cut to form 2 D-shaped samples that were joined by the heat shrink tube. Finally, the samples were dried at 37°C for 24 h. The surface morphology of the substrates was examined to confirm the correct infiltration by scanning electron microscopy (SEM) using a FEI Teneo microscope (FEI, Eindhoven, The Netherlands). Gold sputtering was used to make the surfaces conductive. D-shape samples were observed from the top to check the homogeneity, roughness, and porosity of the coating material. Additionally, the cross section of the D-shaped samples was analyzed to estimate the coating thickness and the degree of infiltration through interconnected porosity. The average pore size of the polymeric composites was evaluated from SEM images using Image-Pro Plus 6.2 software (Mediacibernetic, Bethesda, MD, USA) and the line intercept method.

3. Results and discussion

3.1. Synthesis of PCL/PVA/AgNPs composites

Composites were synthesized with different PCL/PVA ratios and weight percent AgNPs. Materials were named according to the composition of the polymeric blend: 100/0 for the composite containing 100% PCL and 0% PVA; 90/10 for the composite containing 90% PCL and 10% PVA; and so on. In addition, as above mentioned, each blend was mixed with different wt% AgNPs. Fig. S2 provides an overview of some of the prepared composites, organized by polymeric blend composition and amount of AgNPs included (0.1, 0.2, 0.3 and 0.4 wt%). A significant difference in yellowish color was observed when the amount of AgNPs and PVA was increased.

3.2. Antibacterial activity of biopolymer composites

As one of the main aims of this research work, the antibacterial activity of the composites was investigated in two bacterial strains as a reference, gram-negative bacterium, *P. aeruginosa*, and gram-positive bacterium, *S. aureus*, responsible for dental infections as a possible application of these systems. A total of 28 composites were initially tested against *S. aureus* and *P. aeruginosa*. The materials' compositions were the following: PCL/PVA: 100/0, 90/10, 80/20, and 70/30, each one with AgNP in 0.0125%, 0.025%, 0.05%, 0.1%, 0.2%, 0.3% and 0.4%, as shown in Fig. S3. The standardized values of the halos generated by the different samples tested in both bacteria are shown in Fig. 1. As expected, growth inhibition by nanoparticles was dose dependent for both bacteria. In this regard, for *P. aeruginosa*, the minimum amount of AgNP required in the composite to generate inhibition was 0.025%, while for *S. aureus*, the minimum amount was 0.1%, AgNPs. However, the highest antibacterial behavior was observed in the composites prepared with 0.4% AgNPs, in all cases. According to the literature [38–40], the total amount of AgNPs included in these materials is still low enough to be considered in a safe range, avoiding cytotoxicity to the surrounding tissues. Therefore, 0.4% AgNP was selected as the ideal amount of antimicrobial agent to be part of the composites to investigate.

However, another trend was observed in the antibacterial activity of the composites: the higher the proportion of PVA added to the material, the larger the inhibition halo. As shown in Fig. 1, for *P. aeruginosa*, the standardized halo ranged from 1.12 for 100/0 composite with 0.3 wt% AgNPs, the material showing the lower antimicrobial capacity in this bacterial strain, to 1.66 for 70/30 material with 0.4 wt% AgNPs as the composite with higher antibacterial behavior. Likewise, for *S. aureus*, the inhibition halo ranged from 1.03 for the 100/0 composite to 1.71 for the 80/20 material, only slightly higher than the value obtained for the 70/30 composite (1.61). This trend indicated the potential improvement of antimicrobial activity with increasing proportion of PVA in the final composite. For this reason, two other composite materials were added to the investigation: one prepared with 50%–50% PCL/PVA and another with 40%–60% PCL/PVA, both containing 0.4% AgNPs. Antibacterial activity studies were also applied to both materials (Fig. S4). In this case, the standardized inhibition halos measured for the 50/50 composite were 1.71 and 1.83 for *P. aeruginosa* and *S. aureus*, respectively (Fig. 2); while the values calculated from 40/60 were 1.64 and 1.66.

Comparison of the results for inhibition halos obtained for all the composites with 0.4 wt% AgNPs (Fig. 3), revealed that *S. aureus* was, in general, more susceptible to these materials than *P. aeruginosa*. Furthermore, a higher antibacterial activity was found for the 50/50 composite in both bacteria, which points to this material as the

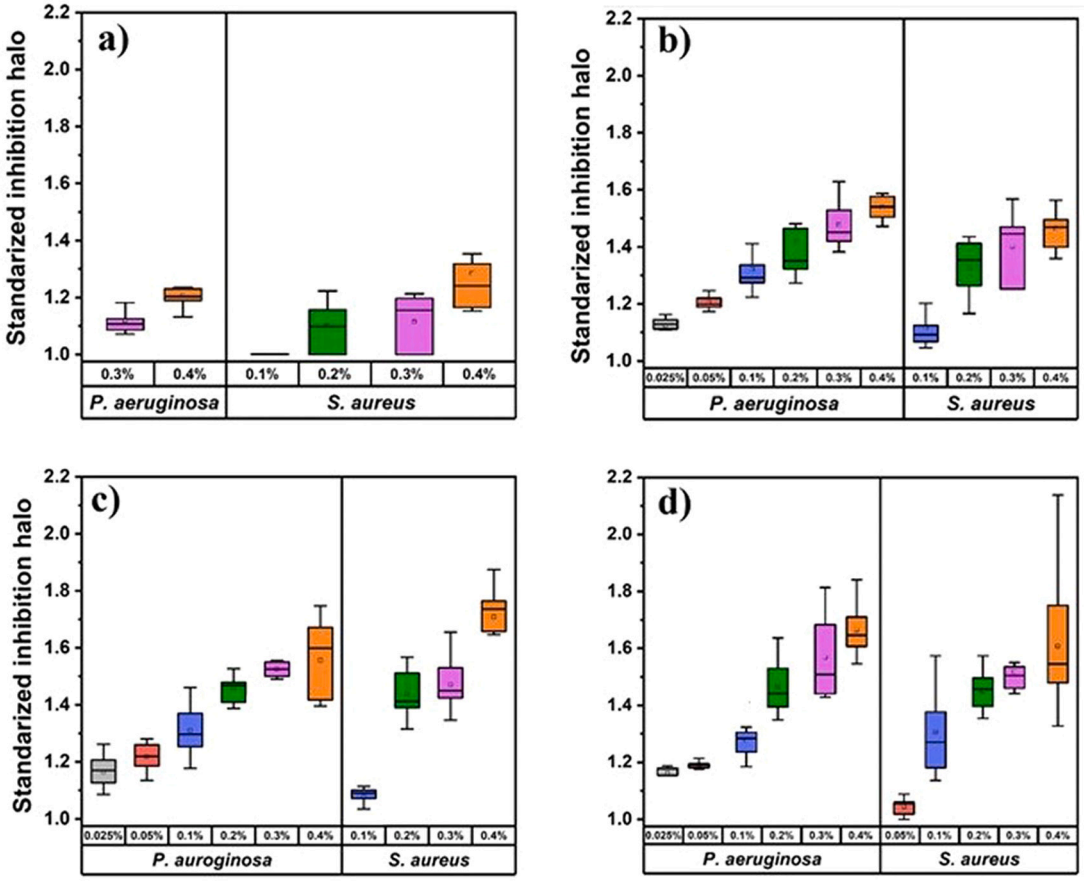

Fig. 1. Standardized values of inhibition halos generated by all composites tested [a) 100/0, b) 90/10, c) 80/20, and d) 70/30]. Note: Materials that did not show inhibition (standardized halo equal or lower than 1) were omitted from the graphics.

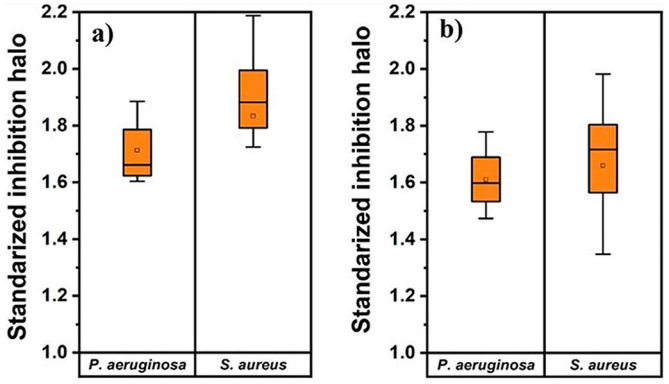

Fig. 2. Standardized values of inhibition halos generated by a) 50/50 and b) 40/60 composites containing 0.4 wt% AgNPs for both bacteria, *P. aeruginosa* and *S. aureus*.

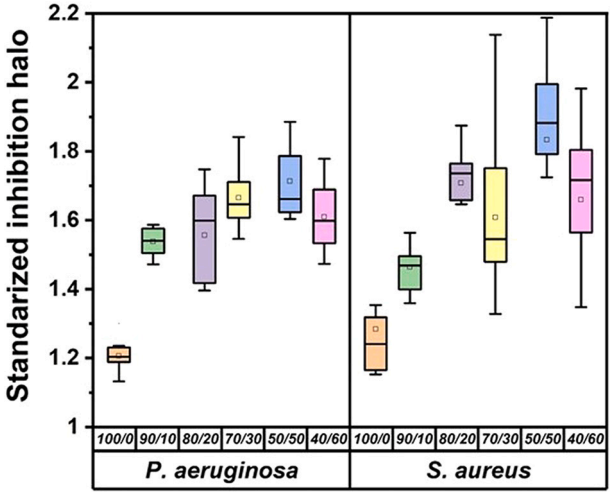

Fig. 3. Comparison of the inhibition areas generated for all composites with 0.4 wt% AgNPs and the two bacterial strains, *P. aeruginosa* and *S. aureus*.

candidate with the best short-term antibacterial properties.

As previously mentioned, silver is known to have multiple activities against *S. aureus*, since it binds to 38 different proteins within the cell [26]. Thus, for example, Wang et al. demonstrated that silver could inhibit the 6-phosphogluconate dehydrogenase through the catalytic His185. Besides, it induces the formation of reactive oxygen species, compromising the integrity of the membrane and inhibiting most of the macromolecular synthetic pathways [27]. Similar mechanisms are reported for *P. aeruginosa*[28]. In addition, the authors have also investigated the role of silver as antimicrobial in a recent publication to elucidate its mechanism of action as a potential therapeutic agent [41].

Some authors have tested the potential of AgNPs as antimicrobial agents in drug release systems. For example, Rodriguez Nuñez et al. [42] investigated the use of PVA and maleic acid as precursors of hydrogels containing AgNPs. Matar et al. [43] developed another AgNP-loaded hydrogel based on locust bean gum and PVA. In both cases, the results obtained after applying a modified version of the Kirby-Bauer method were similar to the ones presented in this manuscript for similar silver concentrations. However, none of them assessed the long-term delivery

of silver, in the form of AgNPs or Ag^+. Probably, the fact of using hydrogels as drug delivery systems may cause a very fast release of silver and therefore a too short prophylactic effect. Madhavan et al. [36] prepared AgNP-impregnated PCL scaffolds. However, they only deposited the nanoparticles on the scaffold surfaces, what would prevent a sustained release of silver throughout the lifetime of the scaffold. On the other hand, many other authors have used PCL and PVA polymers as delivery systems of AgNPs, but they apply these composites always as nanofibers [17,44,45]. This strategy of electrospinning produces entities with a completely different behavior from a pharmaceutical point of view related to the release profile; therefore, they are not comparable to our systems, although chemical composition is quite similar. In addition, most of them use nanoparticles smaller than 10 nm diameter, what drastically increase the toxicity to eukaryotic cells and, again, are not distributed in the same ways as ours.

3.3. Silver release profile

The delivery of Ag to the medium would definitively work as a prophylactic measure and as a therapeutic antimicrobial agent if it were released from the composite in a sustained manner. Therefore, to establish the long-term silver release profile from the different polymeric materials when exposed to water, the presence of Ag^+ was followed by UV–Vis for all composite materials loaded with 0.4% AgNPs. Fig. 4 presents the results obtained in the first 24 h (Fig. 4a) and for the next 20 days (Fig. 4b). The delivery behavior of Ag^+ was similar to that found in other non-swellable matrices, where the release kinetics is described by a two-step process: a first period of surface oxidation of the nanoparticles governed by fickian diffusion and a second step in which the release of ions is ruled by corrosion and polymer degradation that could occur particularly at the grain boundaries in the particle [46]. Therefore, a burst release of Ag^+ was observed for all composites in the first 2–4 h, followed by a more sustained delivery stage that depends on the material. In general, the higher the amount of PCL in the material, the higher the Ag^+ levels observed in the whole experiment. However, while the composites with a higher amount of PCL maintain a sustained release for at least 7 days, materials with more PVA, such as the 40/60 composite, did not show Ag^+ delivery after 6 h. This effect is clearly shown in Table 1, which depicts the cumulative average amounts of Ag^+ detected in 24 h and 21 days with respect to the total AgNPs initially included. Since the mechanisms of action of Ag^+ cations or AgNPs could be different, these results open up the possibility of faster or slower Ag delivery, simply by adjusting the composition of the composite to the particular needs [47].

In summary, a combined antimicrobial effect of both AgNPs and Ag^+ was demonstrated. The Kirby-Bauer experiments showed a greater antibacterial behavior for samples with higher proportions of PVA, what suggests a more important release of AgNPs due to the hydrophilicity of this polymer. This hypothesis was later proved by the Ag^+ measurements, that displayed a higher and more prolonged release of these ions along time in composites with bigger amount of PCL. This fact entails a more elevated entrapment of AgNPs in the composites rich in PCL, a hydrophobic polymer that hinders the release of the nanoparticles, so they have longer times to be oxidized to Ag^+.

Table 1
Average Ag^+ released after 24 h and 21 days

Composites	Ag^+ released in 24 h (%)	Ag^+ released in 21 days (%)
100/0	24.5	31.4
90/10	18.9	22.6
80/20	18.5	20.9
70/30	18.1	20.2
50/50	16.5	17.0
40/60	11.4	11.6

3.4. Infiltration and characterization of coatings onto porous Ti substrate

In previous studies, the authors of this manuscript have reported the advantages of the porous Ti substrates with 50% pore density and 200–355 μm pore size distribution. The substrates characteristics were: $\rho = 2.15$ g/cm^3, $P_T = 51.8\%$, $P_i = 47.5\%$, $D_{eq} = 248$ μm, $F_f = 0.85$, $E_d = 22.9$ GPa and $\sigma_y = 120$ MPa. These values guarantee biomechanical (stiffness and mechanical resistance) and biofunctional (ability to promote bone ingrowth) equilibrium [47–50], as well as allowing infiltration and improving adherence of the different coatings [8,49].

Once the Ti substrates were characterized, two polymeric composites were selected as ideal candidates for their characteristics: the 50/50 composite demonstrated the most elevated short-term antimicrobial activity, with the highest release of AgNPs in the first hours. Meanwhile, among composites with a higher proportion of PCL and therefore a more sustained silver release over time, the 80/20 composite showed the best balance between short- and long-term release. Therefore, a 0.30 g/mL suspension of each composite was infiltrated dropwise onto the porous titanium substrates according to the experimental procedure previously described, letting the samples dry for 24 h at 37°C.

To prove the correct infiltration, SEM images were performed. Fig. 5 shows the good penetration of both composites into the porous material, having a perfect coating over the substrate and excellent anchorage. The uniformity of the coating was demonstrated in Fig. 5a and b, which show a porous honeycomb-shaped structure of the polymer. The thicknesses of these coatings were 61.8 ± 8.5 μm and 90.9 ± 8.4 μm for 50/50 and 80/20 composites, respectively, showing a lower compaction of the materials when the PCL content was higher. The adhesion was confirmed in Fig. 5c and d, where the cross section of the D-shaped infiltrated substrates showed not only the coating layer at the substrate interface but also the composite covering the pores' surface. Indeed, the high interconnected porosity of the Ti samples allowed the coating of the inner pores, as demonstrated in Fig. 5e and f.

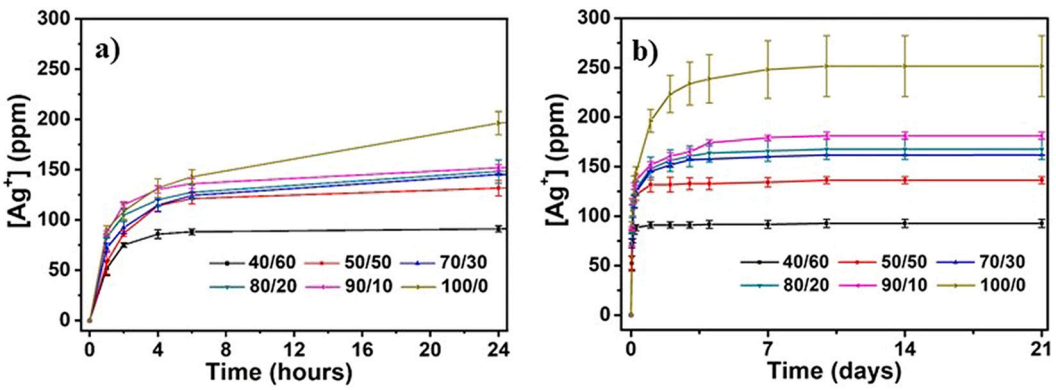

Fig. 4. Cumulative [Ag^+] (ppm) release profiles on different composite materials of PCL/PVA as a function of time: a) first 24 h, b) 21 days.

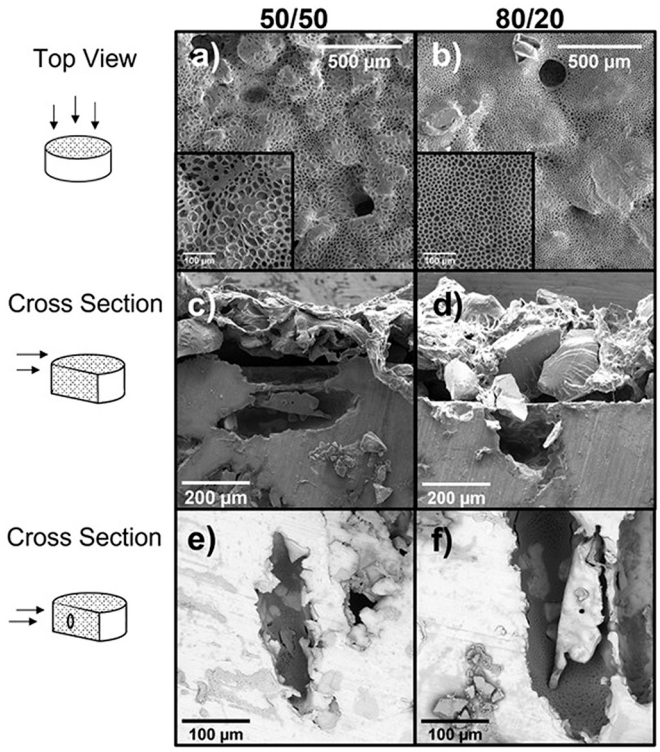

Fig. 5. SEM micrographs of the substrate coating obtained for PCL/PVA 50/50 on the left and 80/20 on the right. Top views are shown in a) and b) and cross section in c) and d). Backscatter SEMs from a porous cross section are represented in e) and f).

In the process of fabricating these coatings, the use of a polar solvent such as dichloromethane with a low evaporation temperature (40°C) was used to completely dissolve the blends. After infiltration of the suspension in porous Ti samples and heating to 37°C in an oven for 24 h, slow gas evaporation occurred to form a thin homogeneous film. Since the dichloromethane gas density is quite high, 2.9 g/mL, compared to other solvents such as water, 1 g/mL, a trapping process of this gas could trigger the honeycomb-like structure of the composite. Also, from the analysis of the appearance of the different polymeric coatings, the pore size of the honeycomb-shaped structure was observed, as depicted in the SEM images shown in Fig. 6. The results confirmed that the 80/20 composite had smaller pores with an average pore size of 14.1 ± 2.9 µm, as given by software image analysis, with narrower mean free path distances between the pores. For a higher amount of PVA (50/50 material), bigger pores were observed, 23.1 ± 5.3 µm, with bigger mean free path distances between these pores. The tendency to pore size was confirmed both by the line intercept method and by average pore sizes, exhibiting values of 14.2 ± 1.0 µm, for 80:20 composite and 25.3 ± 4.2 µm, for the 50/50 samples. The differences observed between the two compositions could be rationalized considering that blends with a high content of PVA form larger pores, perhaps due to their characteristics as a plasticizer, excellent film formation, high tensile strength and flexibility compared to PCL which plays a crucial role in the dichloromethane gas evaporation process. Interestingly, apart from the convenient pore size observed in Ti samples that would enhance the promotion of osseointegration, the pores observed in the polymer-based biomaterial could be considered as an implementation from a biomedical point of view. In this sense, smaller pores (5–15 µm) such as those obtained with the 80/20 composite are known to act promoting fibroblast growth [51]. An interesting aspect that emerged from the analysis of Fig. 6 is that some of the pores contain a small hole at the bottom, which could potentially ensure successful diffusion to the center of titanium samples of nutrients and oxygen to fix proteins and osteoblasts and ease the removal of metabolism waste. Also, this coating topography could influence the degradation process. PCL degrades at a slower rate compared to other FDA approved polymers and has been extensively used in drug delivery systems due to the fact that it could remain active for more than a year. In addition, PVA is a water-soluble material that only biodegrades in the presence of microorganisms or enzymes. Thus, a proper combination of these two polymers may control the preferred degradation rate in the sense that longer clinical antibacterial treatments should include 80/20 composites. On the contrary, 50/50 coatings may appear more appropriate for several weeks of treatments. Furthermore, the formed pore pattern shows high surface per area which may enhance better degradation if compared to plane coatings.

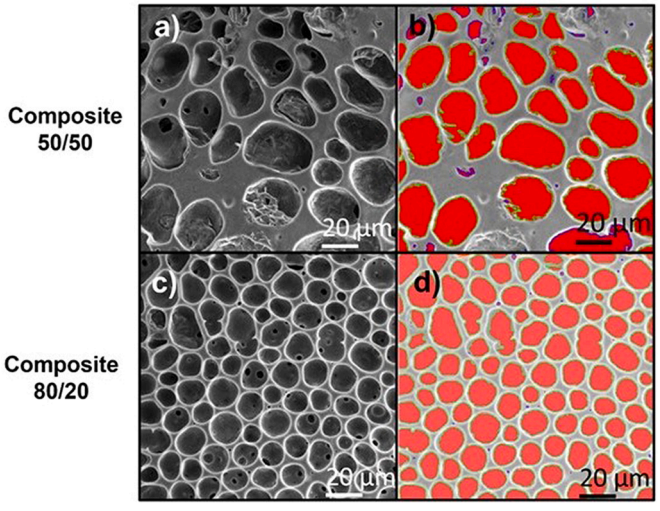

Fig. 6. a) and c) Top-view SEM micrographs of the 50/50 and 80/20 composite coatings, respectively. b) and d) Software image analysis of both coatings, showing the measured pores in red.

Future research should consider the potential synergistic effects of the interconnected Ti pores and the honeycomb-like surface of the polymer coatings to further promote osseointegration and vascularization for implemented implant.

4. Conclusions

In summary, the results of this study describe a simple and affordable approach to the use of AgNPs/PCL/PVA composites as coatings for porous Ti substrates, to provide solutions to common prosthesis problems associated to undesirable infections, stress shielding phenomenon or poor osseointegration.

The fabrication of AgNPs in combination with biocompatible and non-toxic PCL/PVA composites in various proportions has been presented with satisfactory results to be used as prophylactic and versatile coatings for porous Ti samples. Ti's stress shielding phenomenon was minimized via fabrication of substrates using the space-holder technique to get 50% pore density and 200–355 µm pore size distribution. These characteristics provides the required biomechanical equilibrium, good biofunctionality, as well as proper infiltration and adherence of coating. This research work provides new insights, suggesting that both the silver cation and AgNPs released from the composite coating exert an effective antimicrobial behavior against *P. aeruginosa* and *S. aureus*. For this study, 50/50 and 80/20 PCL/PVA composites containing 0.4% AgNPs were selected as short-term or longer-term antimicrobial release models, respectively. In this sense, the 50/50 PCL/PVA polymer composite was capable of generating larger pores (approx. 24 µm) exhibiting stronger short-term antibacterial activity with 7% greater inhibition halos, while the 80/20 material with pores of approximately 14 µm promotes fibroblast growth factor, and displayed better long-term antimicrobial behavior, due to increased sustained release over time (20% more Ag^{+}

released after 21 days).

Author contributions

Investigations, V.G, P.R.-L., V.C.P.G. and BB; analysis of data P.R.-L., V.G., B.B., A.A. and V.C.P.G., microscopy studies; P.R.-L. and V.G., writing—original draft preparation, B.B., V.C.P.G., Y.T., E.P and A.A.; supervision, B.B., A.A and Y.T.; project administration and funding acquisition, E.P., A.A. and Y.T. All authors have read and agreed to the published version of the manuscript.

Funding

This work was supported by the Ministry of Science and Innovation of Spain under the grant PID2019-109371GB-I00 and of the Junta de Andalucía (Spain) through the Projects PAIDI 2020, P20_00671 and FEDER Andalucía US-1380878; together with projects PPI505/2020 and PPI532/2020 (Universidad de Sevilla, Spain).

CRediT authorship contribution statement

Ana Alcudia: Conceptualization, Writing – review & editing, Supervision, Project administration. **Belén Begines:** Conceptualization, Investigation, Writing – review & editing, Supervision. **Paula Rodriguez-Lejarraga:** Investigation, Writing – original draft. **Valeria Greyer:** Investigation, Writing – original draft. **Vanda Cristina Fortio Godinho:** Writing – original draft. **Eloísa Pajuelo:** Supervision. **Yadir Torres:** Conceptualization, Writing – review & editing, Project administration.

Declaration of Competing Interest

The authors declare that they have no known competing financial interests or personal relationships that could have appeared to influence the work reported in this paper.

Acknowledgments

Authors thank the General Services of CITIUS (Universidad de Sevilla) for the help provided.

Appendix A. Supplementary data

Supplementary data to this article can be found online at https://doi.org/10.1016/j.colcom.2022.100621.

References

[1] J.P. Allain, M. Echeverry-Rendón, J.J. Pavón, S.L. Arias, Nanostructured biointerfaces, in: Nanopatterning and Nanoscale Devices for Biological Applications, CRC Press, 2017, pp. 41–72.
[2] M. Wang, T. Tang, Surface treatment strategies to combat implant-related infection from the beginning, J. Orthop. Transl. 17 (2019) 42–54, https://doi.org/10.1016/j.jot.2018.09.001.
[3] K. Pałka, R. Pokrowiecki, Porous titanium implants: a review, Adv. Eng. Mater. 20 (5) (2018) 1–18, https://doi.org/10.1002/adem.201700648.
[4] A. Nouri, P.D. Hodgson, C. Wen, Biomimetic porous titanium scaffolds for orthopedic and dental applications, in: A. Mukherjee (Ed.), Biomimetics Learning from Nature, IntechOpen, 2010, https://doi.org/10.5772/8787.
[5] C.M. Murphy, F.J. O'Brien, Understanding the effect of mean pore size on cell activity in collagen-glycosaminoglycan scaffolds, Cell Adhes. Migr. 4 (3) (2010) 377–381, https://doi.org/10.4161/cam.4.3.11747.
[6] C. Domínguez-Trujillo, F. Ternero, J.A. Rodríguez-Ortiz, J.J. Pavón, I. Montealegre-Meléndez, C. Arévalo, F. García-Moreno, Y. Torres, Improvement of the balance between a reduced stress shielding and bone ingrowth by bioactive coatings onto porous titanium substrates, Surf. Coat. Technol. 338 (2018) 32–37, https://doi.org/10.1016/j.surfcoat.2018.01.019.
[7] A. Barik, N. Chakravorty, Targeted drug delivery from titanium implants: a review of challenges and approaches, Trends Biomed. Res. 1251 (2019) 1–17, https://doi.org/10.1007/5584_2019_447.
[8] C. García-Cabezón, V. Godinho, C. Salvo-Comino, Y. Torres, F. Martín-Pedrosa, Improved corrosion behavior and biocompatibility of porous titanium samples coated with bioactive chitosan-based nanocomposites, Materials (Basel) 14 (21) (2021) 6322, https://doi.org/10.3390/ma14216322.
[9] Y. Jeong, Y. Yao, T.H. Mekonnen, E.K.F. Yim, Changing compliance of poly(vinyl alcohol) tubular scaffold for vascular graft applications through modifying interlayer adhesion and crosslinking density, Front. Mater. 7 (2021) 456, https://doi.org/10.3389/fmats.2020.595295.
[10] S. Roy, S. Kuddannaya, T. Das, H.Y. Lee, J. Lim, X. Hu, Matthew, Y. Chee Yoon, J. Kim, A novel approach for fabricating highly tunable and fluffy bioinspired 3D poly(vinyl alcohol) (PVA) fiber scaffolds, Nanoscale 9 (21) (2017) 7081–7093, https://doi.org/10.1039/C7NR00503B.
[11] M. Jafari, Z. Paknejad, M.R. Rad, S.R. Motamedian, M.J. Eghbal, N. Nadjmi, A. Khojasteh, Polymeric scaffolds in tissue engineering: a literature review, J Biomed Mater Res B Appl Biomater 105 (2) (2017) 431–459, https://doi.org/10.1002/jbm.b.33547.
[12] A.S.K. Kiran, T.S.S. Kumar, R. Sanghavi, M. Doble, S. Ramakrishna, Antibacterial and bioactive surface modifications of titanium implants by PCL/TiO_2 nanocomposite coatings, Nanomaterials (Basel, Switzerland) 8 (10) (2018) 860, https://doi.org/10.3390/nano8100860.
[13] N. Raina, R. Pahwa, J.K. Khosla, P.N. Gupta, M. Gupta, Polycaprolactone-based materials in wound healing applications, Polym. Bull. (2021), https://doi.org/10.1007/s00289-021-03865-w.
[14] L. Ebrahimi, A. Farzin, Y. Ghasemi, A. Alizadeh, A. Goodarzi, A. Basiri, M. Zahiri, A. Monabati, J. Ai, Metformin-loaded PCL/PVA fibrous scaffold preseeded with human endometrial stem cells for effective guided bone regeneration membranes, ACS Biomater. Sci. Eng. 7 (1) (2021) 222–231, https://doi.org/10.1021/acsbiomaterials.0c00958.
[15] S. Mahalingam, C. Bayram, M. Gultekinoglu, K. Ulubayram, S. Homer-Vanniasinkam, M. Edirisinghe, Co-axial gyro-spinning of PCL/PVA/HA core-sheath fibrous scaffolds for bone tissue engineering, Macromol. Biosci. 21 (10) (2021) 1–10, https://doi.org/10.1002/mabi.202100177.
[16] S.B. Abdollahi Boraei, J. Nourmohammadi, B. Bakhshandeh, M.M. Dehghan, H. Gholami, Z. Gonzalez, A.J. Sanchez-Herencia, B. Ferrari, Capability of core-sheath polyvinyl alcohol-polycaprolactone emulsion electrospun nanofibrous scaffolds in releasing strontium ranelate for bone regeneration, Biomed. Mater. 16 (2) (2021) 25009, https://doi.org/10.1088/1748-605X/abdb07.
[17] M.A. Mohamady Hussein, E. Guler, E. Rayaman, M.E. Cam, A. Sahin, M. Grinholc, D. Sezgin Mansuroglu, Y.M. Sahin, O. Gunduz, M. Muhammed, I.M. El-Sherbiny, M. Megahed, Dual-drug delivery of Ag-chitosan nanoparticles and phenytoin via core-shell PVA/PCL electrospun nanofibers, Carbohydr. Polym. 270 (2021) 118373, https://doi.org/10.1016/j.carbpol.2021.118373.
[18] B. Begines, A. Alcudia, R. Aguilera-Velazquez, G. Martinez, Y. He, R. Wildman, M.-J. Sayagues, A. Jimenez-Ruiz, R. Prado-Gotor, Design of highly stabilized nanocomposite inks based on biodegradable polymer-matrix and gold nanoparticles for inkjet printing, Sci. Rep. 9 (1) (2019), https://doi.org/10.1038/s41598-019-52314-2.
[19] B. Begines, T. Ortiz, M. Pérez-Aranda, G. Martínez, M. Merinero, F. Argüelles-Arias, A. Alcudia, Polymeric nanoparticles for drug delivery: recent developments and future prospects, Nanomaterials 10 (7) (2020), https://doi.org/10.3390/nano10071403.
[20] J. Gaviria, A. Alcudia, B. Begines, A.M. Beltrán, J. Villarraga, R. Moriche, J. A. Rodríguez-Ortiz, Y. Torres, Synthesis and deposition of silver nanoparticles on porous titanium substrates for biomedical applications, Surf. Coat. Technol. 406 (2021) 126667, https://doi.org/10.1016/j.surfcoat.2020.126667.
[21] Nanoparticles' Promises and Risks: Characterization, Manipulation, and Potential Hazards to Humanity and the Environment, Springer, 2015.
[22] C. Bankier, R.K. Matharu, Y.K. Cheong, G.G. Ren, E. Cloutman-Green, L. Ciric, Synergistic antibacterial effects of metallic nanoparticle combinations, Sci. Rep. 9 (1) (2019) 16074, https://doi.org/10.1038/s41598-019-52473-2.
[23] R. Rawashdeh, Y. Haik, Antibacterial mechanism of metallic nanoparticles: a review, Dyn. Biochem. Process. Biotechnol. Mol. Biol. 3 (2) (2009) 12–20.
[24] B. Aslam, W. Wang, M.I. Arshad, M. Khurshid, S. Muzammil, M.H. Rasool, M. A. Nisar, R.F. Alvi, M.A. Aslam, M.U. Qamar, M.K.F. Salamat, Z. Baloch, Antibiotic resistance: a rundown of a global crisis, Infect. Drug Resist. 11 (2018) 1645–1658, https://doi.org/10.2147/IDR.S173867.
[25] Z. Xu, C. Zhang, X. Wang, D. Liu, Release strategies of silver ions from materials for bacterial killing, ACS Appl. Bio Mater. 4 (5) (2021) 3985–3999, https://doi.org/10.1021/acsabm.0c01485.
[26] H. Wang, M. Wang, X. Xu, P. Gao, Z. Xu, Q. Zhang, H. Li, A. Yan, R.Y.-T. Kao, H. Sun, Multi-target mode of action of silver against staphylococcus aureus endows it with capability to combat antibiotic resistance, Nat. Commun. 12 (1) (2021) 3331, https://doi.org/10.1038/s41467-021-23659-y.
[27] C.P. Randall, L.B. Oyama, J.M. Bostock, I. Chopra, A.J. O'Neill, The silver cation (Ag+): antistaphylococcal activity, mode of action and resistance studies, J. Antimicrob. Chemother. 68 (1) (2013) 131–138, https://doi.org/10.1093/jac/dks372.
[28] D. Soni, A. Bafana, D. Gandhi, S. Sivanesan, R.A. Pandey, Stress response of Pseudomonas species to silver nanoparticles at the molecular level, Environ. Toxicol. Chem. 33 (9) (2014) 2126–2132, https://doi.org/10.1002/etc.2670.
[29] P. Trueba, A.M. Beltrán, J.M. Bayo, J.A. Rodríguez-Ortiz, D.F. Larios, E. Alonso, D. C. Dunand, Y. Torres, Porous titanium cylinders obtained by the freeze-casting technique: influence of process parameters on porosity and mechanical behavior, Metals (Basel) 10 (2) (2020) 188, https://doi.org/10.3390/met10020188.
[30] ASTM C373–14, Standard Test Method for Water Absorption, Bulk Density, Apparent Porosity, and Apparent Specific Gravity of Fired Whiteware Products, Ceramic Tiles, and Glass Tiles, ASTM International, West Conshohocken, PA, 2014, https://doi.org/10.1520/C0373-14.

[31] International Standard. ISO 13314:2011, Standard for Mechanical Testing of Metals — Ductility Testing — Compression Test for Porous and Cellular Metals, Int. Organ. Stand., Geneva, Switz., 2011.
[32] W.E. Luecke, L. Ma, S.M. Graham, M.A. Adler, Repeatability and Reproducibility of Compression Strength Measurements Conducted According to ASTM E9, 2009, p. 39.
[33] American Society for Testing and Materials. ASTM E9-09, Standard Test Methods of Compression Testing of Metallic Materials at Room Temperature, 2018.
[34] ASM Handbook Vol. 17, Nondestructive Evaluation and Quality Control, ASM International, 1989.
[35] J. Müller-Rochholz, Determination of the elastic properties of lightweight aggregate by ultrasonic pulse velocity measurement, Int. J. Cem. Compos. Light. Concr. 1 (2) (1979) 87–90, https://doi.org/10.1016/0262-5075(79)90014-9.
[36] R.V. Madhavan, M.J. Rosemary, M.A. Nandkumar, K.V. Krishnan, L.K. Krishnan, Silver nanoparticle impregnated poly (ε-caprolactone) scaffolds: optimization of antimicrobial and noncytotoxic concentrations, Tissue Eng. A 17 (3–4) (2011) 439–449, https://doi.org/10.1089/ten.TEA.2009.0791.
[37] CLSI (Ed.), Perfomance Standards for Antimicrobial Disk Susceptibility Tests, 13th ed., Clinical and Laboratory Standards Institute, Wayne, PA, 2018. CLSI Standard M02.
[38] F. Parnia, J. Yazdani, V. Javaherzadeh, S. Maleki Dizaj, Overview of nanoparticle coating of dental implants for enhanced osseointegration and antimicrobial purposes, J. Pharm. Pharm. Sci. 20 (0) (2017) 148–160, https://doi.org/10.18433/J3GP6G.
[39] M. Azizi-Lalabadi, F. Garavand, S.M. Jafari, Incorporation of silver nanoparticles into active antimicrobial nanocomposites: release behavior, analyzing techniques, applications and safety issues, Adv. Colloid Interf. Sci. 293 (2021) 102440, https://doi.org/10.1016/j.cis.2021.102440.
[40] C.A. Dos Santos, M.M. Seckler, A.P. Ingle, I. Gupta, S. Galdiero, M. Galdiero, A. Gade, M. Rai, Silver nanoparticles: therapeutical uses, toxicity, and safety issues, J. Pharm. Sci. 103 (7) (2014) 1931–1944, https://doi.org/10.1002/jps.24001.
[41] C.J. Carrasco, F. Montilla, E. Álvarez, A. Galindo, M. Pérez-Aranda, E. Pajuelo, A. Alcudia, Homochiral imidazolium-based dicarboxylate silver(I) compounds: synthesis, characterisation and antimicrobial properties, Dalt. Trans. 51 (2022) 5061–5071, https://doi.org/10.1039/D1DT04213K.
[42] Y.A.R. Nuñez, R.I. Castro, F.A. Arenas, Z.E. López-Cabaña, G. Carreño, V. Carrasco-Sánchez, A. Marican, J. Villaseñor, E. Vargas, L.S. Santos, E.F. Durán-Lara, Preparation of hydrogel/silver nanohybrids mediated by tunable-size silver nanoparticles for potential antibacterial applications, Polymers (Basel) 11 (4) (2019), https://doi.org/10.3390/polym11040716.
[43] G.H. Matar, M. Andac, Antibacterial efficiency of silver nanoparticles-loaded locust bean gum/polyvinyl alcohol hydrogels, Polym. Bull. 78 (11) (2021) 6095–6113, https://doi.org/10.1007/s00289-020-03418-7.
[44] L. Du, H. Xu, T. Li, Y. Zhang, F. Zou, Fabrication of silver nanoparticle/polyvinyl alcohol/polycaprolactone hybrid nanofibers nonwovens by two-nozzle electrospinning for wound dressing, Fibers Polym. 17 (12) (2016) 1995–2005, https://doi.org/10.1007/s12221-016-6813-0.
[45] L. Du, H.Z. Xu, T. Li, Y. Zhang, F.Y. Zou, Fabrication of ascorbyl palmitate loaded poly(caprolactone)/silver nanoparticle embedded poly(vinyl alcohol) hybrid nanofibre mats as active wound dressings: via dual-spinneret electrospinning, RSC Adv. 7 (50) (2017) 31310–31318, https://doi.org/10.1039/c7ra03193a.
[46] A. Hahn, G. Brandes, P. Wagener, S. Barcikowski, Metal ion release kinetics from nanoparticle silicone composites, J. Control. Release 154 (2) (2011) 164–170, https://doi.org/10.1016/j.jconrel.2011.05.023.
[47] B. Reidy, A. Haase, A. Luch, K.A. Dawson, I. Lynch, Mechanisms of silver nanoparticle release, transformation and toxicity: a critical review of current knowledge and recommendations for future studies and applications, Materials (Basel) 6 (6) (2013) 2295–2350, https://doi.org/10.3390/ma6062295.
[48] Y. Torres, B. Begines, A.M. Beltrán, A.R. Boccaccini, Deposition of bioactive gelatin coatings on porous titanium: influence of processing parameters, size and pore morphology, Surf. Coat. Technol. 421 (2021) 127366, https://doi.org/10.1016/j.surfcoat.2021.127366.
[49] A.M. Beltrán, B. Begines, A. Alcudia, J.A. Rodríguez-Ortiz, Y. Torres, Biofunctional and tribomechanical behavior of porous titanium substrates coated with a bioactive glass bilayer (45S5–1393), ACS Appl. Mater. Interfaces 12 (27) (2020), https://doi.org/10.1021/acsami.0c07318.
[50] A. Civantos, C. Domínguez, R.J. Pino, G. Setti, J.J. Pavón, E. Martínez-Campos, F. J. Garcia Garcia, J.A. Rodríguez, J.P. Allain, Y. Torres, Designing bioactive porous titanium interfaces to balance mechanical properties and in vitro cells behavior towards increased osseointegration, Surf. Coat. Technol. 368 (2019) 162–174, https://doi.org/10.1016/j.surfcoat.2019.03.001.
[51] Y. Xia, J. Sun, L. Zhao, F. Zhang, X.-J. Liang, Y. Guo, M.D. Weir, M.A. Reynolds, N. Gu, H.H.K. Xu, Magnetic field and nano-scaffolds with stem cells to enhance bone regeneration, Biomaterials 183 (2018) 151–170, https://doi.org/10.1016/j.biomaterials.2018.08.040.